Research Article | Vol. 26, No. 16 | 6 Aug 2018 | OPTICS EXPRESS 19864
Optics EXPRESS

Multi-modal chip-based fluorescence and quantitative phase microscopy for studying inflammation in macrophages

VISHESH DUBEY,[1,2] AZEEM AHMAD,[1,2] RAJWINDER SINGH,[2,4] DEANNA L WOLFSON,[2] PURUSOTAM BASNET,[3] GANESH ACHARYA,[3,5] DALIP SINGH MEHTA,[1,6] AND BALPREET SINGH AHLUWALIA[2,*]

[1]*Applied Optics and Biophotonics Laboratory, Department of Physics, Indian Institute of Technology Delhi, India*
[2]*Department of Physics and Technology, UiT The Arctic Univ. of Norway, Norway*
[3]*Department of Clinical Medicine, UiT The Arctic Univ. of Norway, Norway*
[4]*Cell Biology and Biophysics Unit, EMBL Heidelberg, Germany*
[5]*Department of Clinical Science, Intervention and Technology Karolinska Univ. Hospital, Sweden*
[6]*mehtads@physics.iitd.ac.in*
[*]*balpreet.singh.ahluwalia@uit.no*

Abstract: Total internal reflection fluorescence (TIRF) microscopy benefits from high-sensitivity, low background noise, low photo-toxicity and high-contrast imaging of sub-cellular structures close to the membrane surface. Although, TIRF microscopy provides high-contrast imaging it does not provide quantitative information about morphological features of the biological cells. Here, we propose an integrated waveguide chip-based TIRF microscopy and label-free quantitative phase imaging (QPI). The evanescent field present on top of a waveguide surface is used to excite the fluorescence and an upright microscope is used to collect the signal. The upright microscope is converted into a Linnik-type interferometer to sequentially extract both the quantitative phase information and TIRF images of the cells. Waveguide chip-based TIRF microscopy benefits from decoupling of illumination and collection light path, large field of view imaging and pre-aligned configuration for multi-color TIRF imaging. The proposed multi-modal microscopy is used to study inflammation caused by lipopolysaccharide (LPS) on rat macrophages. The TIRF microscopy showed that LPS inflammatory molecule disrupts the cell membrane and causes cells to significantly expand across a substrate. While, QPI module quantified changes in the sub-cellular content of the LPS challenged macrophages, showing a net decrease in its maximum phase values.

OCIS codes: (180.4243) Near-field microscopy; (130.0130) Integrated optics; (180.2520) Fluorescence microscopy; (170.3880) Medical and biological imaging.

References and links

1. M. Mir, B. Bhaduri, R. Wang, R. Zhu, and G. Popescu, "Quantitative phase imaging," Prog. Opt. **57**, 133–217 (2012).
2. D. Axelrod, "Total internal reflection fluorescence microscopy in cell biology," Traffic **2**(11), 764–774 (2001).
3. B. O. Leung and K. C. Chou, "Review of super-resolution fluorescence microscopy for biology," Appl. Spectrosc. **65**(9), 967–980 (2011).
4. K. Lee, K. Kim, J. Jung, J. Heo, S. Cho, S. Lee, G. Chang, Y. Jo, H. Park, and Y. Park, "Quantitative phase imaging techniques for the study of cell pathophysiology: from principles to applications," Sensors (Basel) **13**(4), 4170–4191 (2013).
5. V. Dubey, G. Singh, V. Singh, A. Ahmad, and D. S. Mehta, "Multispectral quantitative phase imaging of human red blood cells using inexpensive narrowband multicolor LEDs," Appl. Opt. **55**(10), 2521–2525 (2016).
6. C. Burch and J. Stock, "Phase-contrast microscopy," J. Sci. Instrum. **19**(5), 71–75 (1942).
7. D. B. Murphy and M. W. Davidson, "Differential interference contrast microscopy and modulation contrast microscopy," *Fundamentals of Light Microscopy and Electronic Imaging*, 2nd ed. 173–197 (2012).
8. A. Ahmad, V. Dubey, G. Singh, V. Singh, and D. S. Mehta, "Quantitative phase imaging of biological cells using spatially low and temporally high coherent light source," Opt. Lett. **41**(7), 1554–1557 (2016).

#324513 https://doi.org/10.1364/OE.26.019864
Journal © 2018 Received 19 Feb 2018; revised 10 May 2018; accepted 14 May 2018; published 24 Jul 2018

Optics EXPRESS

9. P. Marquet, B. Rappaz, P. J. Magistretti, E. Cuche, Y. Emery, T. Colomb, and C. Depeursinge, "Digital holographic microscopy: a noninvasive contrast imaging technique allowing quantitative visualization of living cells with subwavelength axial accuracy," Opt. Lett. **30**(5), 468–470 (2005).
10. C. J. Mann, P. R. Bingham, H. K. Lin, V. C. Paquit, and S. S. Gleason, "Dual modality live cell imaging with multiple-wavelength digital holography and epi-fluorescence," 3D Res. **2**, 5 (2011).
11. B. Rappaz, P. Marquet, E. Cuche, Y. Emery, C. Depeursinge, and P. Magistretti, "Measurement of the integral refractive index and dynamic cell morphometry of living cells with digital holographic microscopy," Opt. Express **13**(23), 9361–9373 (2005).
12. L. V. Johnson, M. L. Walsh, B. J. Bockus, and L. B. Chen, "Monitoring of relative mitochondrial membrane potential in living cells by fluorescence microscopy," J. Cell Biol. **88**(3), 526–535 (1981).
13. J. Zhang, R. E. Campbell, A. Y. Ting, and R. Y. Tsien, "Creating new fluorescent probes for cell biology," Nat. Rev. Mol. Cell Biol. **3**(12), 906–918 (2002).
14. A. Diaspro, G. Chirico, and M. Collini, "Two-photon fluorescence excitation and related techniques in biological microscopy," Q. Rev. Biophys. **38**(2), 97–166 (2005).
15. J. G. White, W. B. Amos, and M. Fordham, "An evaluation of confocal versus conventional imaging of biological structures by fluorescence light microscopy," J. Cell Biol. **105**(1), 41–48 (1987).
16. J. S. Burmeister, L. A. Olivier, W. M. Reichert, and G. A. Truskey, "Application of total internal reflection fluorescence microscopy to study cell adhesion to biomaterials," Biomaterials **19**(4-5), 307–325 (1998).
17. H. Schneckenburger, "Total internal reflection fluorescence microscopy: technical innovations and novel applications," Curr. Opin. Biotechnol. **16**(1), 13–18 (2005).
18. H. M. Grandin, B. Städler, M. Textor, and J. Vörös, "Waveguide excitation fluorescence microscopy: A new tool for sensing and imaging the biointerface," Biosens. Bioelectron. **21**(8), 1476–1482 (2006).
19. A. L. Stout and D. Axelrod, "Evanescent field excitation of fluorescence by epi-illumination microscopy," Appl. Opt. **28**(24), 5237–5242 (1989).
20. Z. Liu, L. D. Lavis, and E. Betzig, "Imaging live-cell dynamics and structure at the single-molecule level," Mol. Cell **58**(4), 644–659 (2015).
21. A. L. Mattheyses, S. M. Simon, and J. Z. Rappoport, "Imaging with total internal reflection fluorescence microscopy for the cell biologist," J. Cell Sci. **123**(21), 3621–3628 (2010).
22. C. S. Yelleswarapu, M. Tipping, S.-R. Kothapalli, A. Veraksa, and D. V. Rao, "Common-path multimodal optical microscopy," Opt. Lett. **34**(8), 1243–1245 (2009).
23. X. Quan, K. Nitta, O. Matoba, P. Xia, and Y. Awatsuji, "Phase and fluorescence imaging by combination of digital holographic microscopy and fluorescence microscopy," Opt. Rev. **22**(2), 349–353 (2015).
24. S. Ramachandran, D. A. Cohen, A. P. Quist, and R. Lal, "High performance, LED powered, waveguide based total internal reflection microscopy," Sci. Rep. **3**(1), 2133 (2013).
25. M. L. Martin-Fernandez, C. J. Tynan, and S. E. Webb, "A 'pocket guide' to total internal reflection fluorescence," J. Microsc. **252**(1), 16–22 (2013).
26. K. N. Fish, "Total internal reflection fluorescence (TIRF) microscopy," Curr. Protoc. Cytom. **50**(1)12–18 (2009).
27. J.-C. Tinguely, Ø. I. Helle, and B. S. Ahluwalia, "Silicon nitride waveguide platform for fluorescence microscopy of living cells," Opt. Express **25**(22), 27678–27690 (2017).
28. B. Agnarsson, S. Ingthorsson, T. Gudjonsson, and K. Leosson, "Evanescent-wave fluorescence microscopy using symmetric planar waveguides," Opt. Express **17**(7), 5075–5082 (2009).
29. B. Agnarsson, A. B. Jonsdottir, N. B. Arnfinnsdottir, and K. Leosson, "On-chip modulation of evanescent illumination and live-cell imaging with polymer waveguides," Opt. Express **19**(23), 22929–22935 (2011).
30. A. Hassanzadeh, M. Nitsche, S. Mittler, S. Armstrong, J. Dixon, and U. Langbein, "Waveguide evanescent field fluorescence microscopy: Thin film fluorescence intensities and its application in cell biology," Appl. Phys. Lett. **92**(23), 233503 (2008).
31. B. Agnarsson, A. Lundgren, A. Gunnarsson, M. Rabe, A. Kunze, M. Mapar, L. Simonsson, M. Bally, V. P. Zhdanov, and F. Höök, "Evanescent Light-Scattering Microscopy for Label-Free Interfacial Imaging: From Single Sub-100 nm Vesicles to Live Cells," ACS Nano **9**(12), 11849–11862 (2015).
32. B. Agnarsson, A. B. Jonsdottir, N. B. Arnfinnsdottir, and K. Leosson, "On-chip modulation of evanescent illumination and live-cell imaging with polymer waveguides," Opt. Express **19**(23), 22929–22935 (2011).
33. R. Diekmann, Ø. I. Helle, C. I. Øie, P. McCourt, T. R. Huser, M. Schüttpelz, and B. S. Ahluwalia, "Chip-based wide field-of-view nanoscopy," Nat. Photonics **11**(5), 322–328 (2017).
34. S. N. Vogel, S. T. Marshall, and D. L. Rosenstreich, "Analysis of the effects of lipopolysaccharide on macrophages: differential phagocytic responses of C3H/HeN and C3H/HeJ macrophages in vitro," Infect. Immun. **25**(1), 328–336 (1979).
35. S. M. Lindecrantz and O. G. Hellesø, "Estimation of propagation losses for narrow strip and rib waveguides," IEEE Photonics Technol. Lett. **26**(18), 1836–1839 (2014).
36. Y. K. Jaiswal, M. K. Jaiswal, V. Agrawal, and M. M. Chaturvedi, "Bacterial endotoxin (LPS)-induced DNA damage in preimplanting embryonic and uterine cells inhibits implantation," Fertil. Steril. **91**(5 Suppl), 2095–2103 (2009).

Optics EXPRESS

1. Introduction

High-resolution fluorescence microscopy and quantitative phase imaging of the specimen provide important information about biological processes [1–4]. The scattering or absorption of the light from most of the biological samples is relatively weak when the refractive index of cells is close to that of the surrounding environment [4,5]. It is therefore difficult to get a high contrast image of cells using bright field optical microscopy. This has lead to widespread usage of optical microscopy techniques that can generate high-contrast images. The two most common techniques to enhance the contrast of the sample are a) phase enhanced label-free optical microscopy and b) fluorescence based optical microscopy.

For label free microscopy, phase contrast (PC) and differential interference contrast (DIC) microscopy techniques are widely employed [6,7]. Although PC and DIC microscopy techniques enable visualization of cells, these techniques only provide qualitative information. To quantify the information associated with the morphological features, several interferometry techniques have been developed [1,5,8]. In particular digital holographic microscopy (DHM) is a popular technique commonly employed for 3D measurement of the object by combining interferometry technique with computation post processing [1,9,10]. The amplitude and phase information of the object is encoded in the hologram and is extracted by the inverse optical wave propagation. DHM is a single shot technique enabling high-speed imaging and is therefore widely used for live cell imaging applications, such as cell membrane fluctuations, cell growth and cell division [9,11].

The availability of different labeling strategies has allowed fluorescence microscopy to be applied extensively for studying sub-cellular molecular events and functional mapping of the cells [3,12]. Different sub-cellular components such as nucleus, cell membrane, lysosomes, mitochondria etc. can be labeled with high specificity. There are several variants of fluorescence microscopic techniques, such as confocal fluorescence, total internal reflection fluorescence (TIRF), two-photon and multi-photon absorption fluorescence techniques, each providing its own distinct advantages [10,12–15]. TIRF microscopy is predominately employed for investigating biological phenomena close to the membrane surface [2,16–18]. TIRF microscopy uses an evanescent field that decays exponentially from the surface to illuminate a thin section of the cell (typically less than 200 nm) [16,18]. In epifluorescence, the illumination extends through the entire bulk of the specimen, generating fluorescence signal from the entire specimen. The photons that are emitted by fluorophores well beyond the focal plane contributes towards the background noise. The inefficient mode of illumination and emitted photons contributes in premature bleaching of the labeled molecules and also enhanced phototoxicity [19–21]. While in TIRF-M, the exponentially decaying evanescent field only illuminates a thin section of the cell (typically upto 200 nm). As fluorophores residing beyond the reach of the evanescent field are not illuminated, the TIRF-M generates images with excellent signal to noise (i.e. low background noise). Therefore, the total exposure of light dosage to the cell is less in TIRF-M as compared to the epi-fluorescence, which results in less phototoxicity [19,21]. In contrast to wide-field epi-fluorescence, TIRF provides extremely high contrast images of the biological processes occurring near the cell membrane and also reduces cellular photo-damage and light bleaching [19,21].

In cell biology, both fluorescence and label-free QPI are routinely used to study different properties of the specimen under investigation. Fluorescence microscopy provides morphological information of the specimen with excellent specificity, while phase microscopy provides quantitative information of the specimen. However, fluorescence and QPI techniques are typically used separately, thus lacking multi-modality. There have been only a few proposed methods to combine the advantages of both phase and wide-field fluorescence microscopy for simultaneous measurement [10,22,23]. However, to the best of our knowledge, the integration of TIRF microscopy with QPI has not been performed so far. Integration of TIRF microscopy with QPI will be beneficial for imaging biological events

Optics EXPRESS

close to the membrane surface (such as focal adhesion points, cell-substrate interfaces) using a TIRF module and sequential measurement of the quantitative information about the morphology of the specimen using a phase module.

In this work, we propose integrated waveguide chip-based TIRF microscopy and Linnik-type interferometric QPI for multimodal imaging of the biological specimen. The total internal reflection (TIR) phenomenon were achieved through different optical arrangements; some uses a high numerical aperture (NA>1.4) objective lens and others use a prism configuration. The use of a sufficiently high NA objective, supercritical angle can be achieved for TIR illumination [2,19]. Prism-based TIR has also been used to generate evanescent field but the bulky prism restricts the sample movement and sample mounting schemes. Moreover, the evanescent field generated by prism is only confined in one dimension (in vertical axis) [2,24]. Here, instead of using a specialized high numerical aperture TIRF objective lens, a waveguide chip is used to both hold the sample and to illuminate the sample using the evanescent field present on top of a waveguide surface [18,25,26]. In chip-based TIRF microscopy the generation of the evanescent field on the top of waveguide surface is independent of the objective lens, which exhibits several advantages compared to conventional TIRF systems. Contrary, to prism-based set-up, the evanescent field generated by the waveguide-chip is confined in two dimensions enabling generations of different sets of illumination patterns and integration with other integrated on-chip optical functions. Moreover, it is a compact experimental-setup circumventing the need of expensive TIRF lens [27–31] and pre-aligned set-up for easy multi-color TIRF imaging without additional optical alignment and mechanical adjustments. Moreover, a waveguide chip-based TIRF microscopy has been employed for the imaging of living samples [27,29,32]. Recently, super-resolution microscopy (nanoscopy) based on single molecule localization microscopy was demonstrated using evanescent field excitation from the optical waveguide. It was demonstrated that chip-based optical nanoscopy benefits from the extraordinarily large field-of-view (FOV) as compared to conventional optical nanoscopy [31,34].

Similarly, the integration of the chip-based TIRF microscopy with QPI benefits from a) decoupled illumination light path for the TIRF and the phase modules, b) easy of changing the magnification of the imaging objective lens without influencing the TIRF module; c) TIRF and QPI images over extended FOV and d) compact experimental set-up. The multi-modal microscopy enabled to acquire both TIRF and QPI images on the same experimental set-up, immediately after one another without the need of removing the sample between two microscopy platforms, i.e. TIRF and QPI. Since, the experiment is performed on the live cells, it is therefore preferred to acquire both TIRF and QPI of the same FOV at the same (or almost similar) time points. If two separate set-ups are used to acquire TIRF and QPI images then it is difficult to get same temporal resolution as achieved by using integrated set-up. Moreover, it will also be challenging to swiftly find same cells on two different set-ups, further reducing the temporal resolution.

Using the proposed multi-modal microscopy, the TIRF imaging of the live cells were obtained to study the morphological and the functional features of the cells, while the quantitative phase information was obtained using an off-axis hologram with large spatial carrier frequency captured by a Linnik-type interferometry . The real-time holograms were reconstructed using Fourier transform fringe analysis. The set-up was further employed for the multi-modal imaging of macrophages under normal and inflammated conditions. The multi-modal microscope was used to study the changes in functional and morphological features in macrophages during externally induced inflammation caused by lipopolysaccharide (LPS), an inflammation inducing molecule.

Optics EXPRESS

2. Theory

2.1. Principle of TIRF microscopy

On-chip TIRF microscopy exploits the evanescent field generated by the laser light total internally reflected inside a waveguide. Total internal reflection (TIR) phenomenon occurs when the incidence angle exceeds the critical angle when light travels from a high refractive index (RI) medium into a lower RI medium [2,16]. The critical angle (θ_c) defined by the higher RI (waveguide in our case) of the incident medium (n_1) and the lower RI of a semi-infinite homogeneous solution where sample is kept (n_2) as [16,17]

$$\theta_c = \sin^{-1}\left(n_2 / n_1\right) \tag{1}$$

The evanescent field is generated upon TIR of the light at the interface. The intensity of the evanescent field exponentially decays in z (perpendicular to the interface) direction and is expressed as

$$I_e(z) = I_0 \exp\left(-z/d\right) \tag{2}$$

where I_0 is the incident intensity at the interface and d is the characteristic depth of penetration given by

$$d = \frac{\lambda}{4\pi\sqrt{n_1^2 \sin^2\theta - n_2^2}} \tag{3}$$

where λ is the wavelength of incident light and θ is the angle of incidence [16,17].

2.2. Principle of quantitative phase imaging

We have integrated a waveguide based TIRF microscope with Linnik type interferometric microscopy for multi-modal imaging of specimens. The proposed configuration provides the quantitative information of the phase delay produced by an object without introducing any external reagent. In this interferometric configuration, light from a laser source is divided into two beams; one beam propagates towards a reference mirror and another beam interacts with the sample. The light reflected from the reference mirror and the light backscattered from the sample combine at the beam splitter, thus producing an interference pattern. The illumination is wide field and a sufficient angle is introduced between the two beams to produce a large spatial carrier frequency of fringes, referred to as a digital off-axis hologram, which is recorded by CCD/CMOS camera. The digital off-axis hologram *H(x, y)* can be expressed as the summation of the reference and object wave as [1,9,23]:

$$H(x,y) = \left|E_r(x,y) + E_s(x,y)\right|^2 \tag{4}$$

$$= \left|E_r(x,y)\right|^2 + \left|E_s(x,y)\right|^2 + \left|E_s(x,y)\right|\left|E_r^*(x,y)\right|\exp\left[i\left(\phi(x,y)\right)\right] \tag{5}$$

where $E_r(x, y)$ and $E_s(x, y)$ are the field distribution of reference and sample, and ϕ(x, y) is the spatially varying phase associated with the sample. Two-dimensional Fourier transform (FT) fringe analysis was used for reconstructing the phase map of object. The details of this method can be found elsewhere [1,9]. Fourier transform fringe analysis is a single shot method in which a single interferogram is required to extract the phase of the light field. After computing the FT of the hologram and looking at the spectrum profile, it is easy to isolate one of the cross correlation terms. The filtered cross correlation term is shifted to center and then inverse Fourier transformed to obtain the complex field information of the specimen and defined as $H_{filt} = \left|E_s(x,y)\right|\left|E_r^*(x,y)\right|\exp\left[i\phi(x,y)\right]$ term. The resulting complex information

Optics EXPRESS

can be further utilized for the calculation of phase delay introduced due to the sample as follows [1,9]:

$$\phi(x,y) = \arctan\frac{\mathrm{Im}\left(H_{filt}(x,y)\right)}{\mathrm{Re}\left(H_{filt}(x,y)\right)} \tag{6}$$

where $Im(H_{filt})$ and $Re(H_{filt})$ shows the imaginary and real part of the inverse Fourier transformed term, respectively. The reconstructed wrapped phase map value lies between $-\pi$ to $+\pi$, which is further corrected by a two-dimensional (2D) phase unwrapping algorithm [5,8].

The reconstructed phase map (Eq. (6)), is carrying the information about the object height and refractive index variation which can be determined utilizing the formula [5,8]

$$\phi(x,y) = \frac{2\pi}{\lambda}\left(n_s(x,y) - n_m(x,y)\right) * 2h(x,y) \tag{7}$$

where $n_s(x, y)$ and $n_m(x, y)$ represents the RI of sample and medium respectively and $h(x, y)$ is the geometrical thickness of sample.

3. Material and method

3.1 Experimental setup

The schematic diagram of the integrated chip-based TIRF microscopy and QPI is shown in Fig. 1. A Linnik-type interference microscopy setup is used to record the off-axis hologram, while a waveguide based TIRF imaging setup is used to record the fluorescent images (in green dotted box). All of the optical lenses (L_1-L_6), beam splitters (BS_1-BS_3), single mode fiber (SMF) and mirrors (M_1-M_2) utilized in the experimental setup were imported from Thorlabs. The microscope objectives lenses (MO_1-MO_4) are from Olympus and the emission and band pass filters were bought from Edmund Optics. The focal lengths of the lenses L_1 to L_6 are 25mm, 100mm, 75mm, 150mm, 100mm and 200mm, respectively. For TIRF imaging the laser light is coupled into the waveguide using objective lens MO_1 (40X, 0.65 N.A.). This coupling objective was attached on a piezo controlled three-axis stage to maximize the light coupling into the waveguide. The excitation lasers of 480 nm and 660 nm were used for TIRF imaging. A suitable fluorescent filter set was used to avoid collecting scattered light during image acquisition. The laser beams propagate through a waveguide by TIR phenomenon. The evanescent field generated on the top of the waveguide is used to excite the fluorophores near to the waveguide surface. The waveguide was made of tantalum pentoxide (Ta_2O_5), a high RI material with RI = 2.1 [27,33]. High-refractive index material enables tight confinement of light inside the waveguide and by fabricating thin waveguides (100-200 nm thick), the intensity in the evanescent field on top of the waveguide surface can be enhanced [27,33]. Firstly, a thin layer (around 200 nm thick) of Ta_2O_5 material was deposited using magnetron sputtering onto a silicon dioxide (SiO_2) substrate. The sputtering parameters such as substrate temperature, magnetron power and the oxygen flow rate were optimized using an iterative process. The optimized parameters chosen were 200°C substrate temperature, magnetron power of 300 W and O_2 and Ar flow rates of 5 and 20 sccm, respectively. Standard photolithography followed by ion-beam milling was used to fabricate the waveguides. A rib waveguide was fabricated by only partially etching down the Ta_2O_5 layer. A 50 μm wide rib waveguide with a rib height of 100 nm and total height of 200 nm was used to perform the experiment. The sidewall roughness that contributes towards the propagation losses were reduced by optimization of the ion-beam milling process. The plasma etching was performed to remove the remaining photoresist from the photolithography step. This was followed by post-fabrication annealing for 5 hours at 600°C to further reduce the propagation losses [35].

Optics EXPRESS

For QPI, a He-Ne laser (λ~632nm, power~5 mW) is used to record interferograms. The laser light was coupled into a single mode fiber using 20X (0.40 N.A.) objective lens MO_2. The light from the fiber is then collimated and again focused on the back-focal plane of the objective lens MO_3 (60X, water immersed, NA = 1.2) in the sample arm. Using this arrangement, the object is illuminated by a collimated beam to avoid phase errors due to converging or diverging illumination. The reflected beams from the sample as well as the reference mirror are combined at the beam splitter. Finally, a spatially modulated hologram of a sample is captured using a high speed CMOS (Hamamatsu ORCA-Flash4.0 LT, C11440-42U) image sensor. The typical exposure time for the QPI and TIRF-M is 30 ms and 100 ms, respectively. Further, Fourier transform based image post processing was done to retrieve the phase information about the specimen.

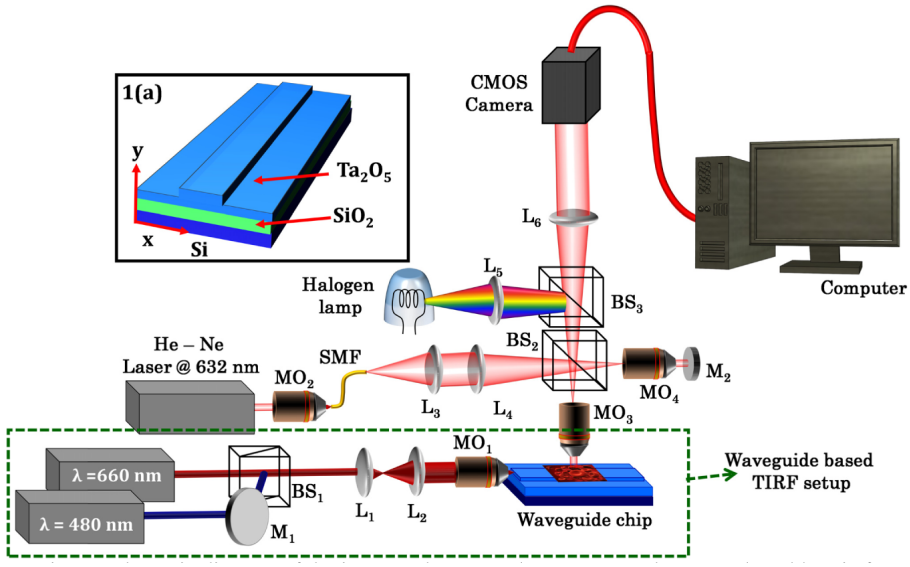

Fig. 1. Schematic diagram of the integrated TIRF and QPI setup. The green dotted box is for TIRF imaging module and sample is positioned on the top surface of waveguide (BS- Beam-splitter, L- lens, MO-microscope objective, SMF-single mode fiber). Figure 1(a) shows the schematic diagram of Ta_2O_5 rib waveguide geometry on Si substrate.

3.2 Preparation of biological samples

RAW 264.7 (rat macrophages) and MCC13 (Merkel cell carcinoma cell line from human skin) cells were maintained in standard culture conditions at 37°C in a humidified 5% CO_2 incubator. The culture medium used was RPMI 1640, supplemented with 10% fetal calf serum (FCS) and 1% penicillin/streptomycin. The cells were divided when they reached 80-90% confluency, approximately every 2-3 days. Cellmask Green (CMG), Cellmask Deep Red (CMDR) and culture medium RPMI 1640 were bought from Thermofisher Scientific.

For stimulation studies, RAW 264.7 cells were seeded into a PDMS chamber on the fibronectin-coated waveguide at 10^5 cells/mL concentration. The cells were then incubated overnight. The next day, cell samples on waveguides were divided into two sets. Culture media from one set was replaced with 10μg/mL of lipopolysaccharide (LPS) dissolved in culture media. The media of the other set of samples was replaced with fresh culture media as a control. The samples were again incubated for 24 hour and post-incubation the samples were washed twice with pre-warmed RPMI. For labeling, Cellmask Green (CMG) was diluted from stock solution (1mM) to a final concentration of 1:1000 in complete media. The

Optics EXPRESS

samples were incubated with the CMG for 10 minutes, then washed twice with RPMI media and mounted in complete media once again for imaging.

MCC13 cells were seeded onto waveguides 24 hours prior to labeling. For TIRF imaging, cells were washed twice with RPMI before labeling with 1:1000 dilution of Cellmask Deep Red (CMDR) in RPMI for 10 minutes. Cells were washed twice before imaging.

4. Results and discussion

4.1 Spatial-temporal resolution of the system (phase module)

In order to determine phase sensitivity, the assessment of the temporal and the spatial phase noise is important for the QPI technique that also establishes the stability of the setup. To measure the phase noise, a time-lapsed movie of interference was acquired for a minute by placing a standard flat mirror (surface flatness of λ/10 over 1 inch diameter) on the sample and the reference arms under the stable environmental conditions. Figure 2(a) shows the interferogram recorded with mirror, Fig. 2(b) shows the spatial noise of the system at a single time point. The color bar corresponds to phase (in mrad) and the x and y axis having pixel values. Figure 2(c) shows the temporal noise of the setup with respect to time. The average spatial and temporal noise of the proposed setup was determined to be approximately 50 mrad. The spatial phase sensitivity of the QPM system is measured using unstructured Si substrate as a test specimen and found to be comparable to the standard flat mirror. In addition, Si substrate is preferred for phase noise measurement because the waveguide structures were fabricated on similar type of Si substrate. For the precision in height measurement of QPM setup, we performed experiment on the strip waveguide of different height of 8nm, 20 nm, and 50nm. We observe that the height map up to 20 nm is not resolved (not shown here) and the height of 50 nm is clearly resolved by utilizing proposed QPM system as shown in Fig. 2 (f). Therefore, the intrinsic precision in height measurement is approx. greater than 20 nm and less than 50 nm.

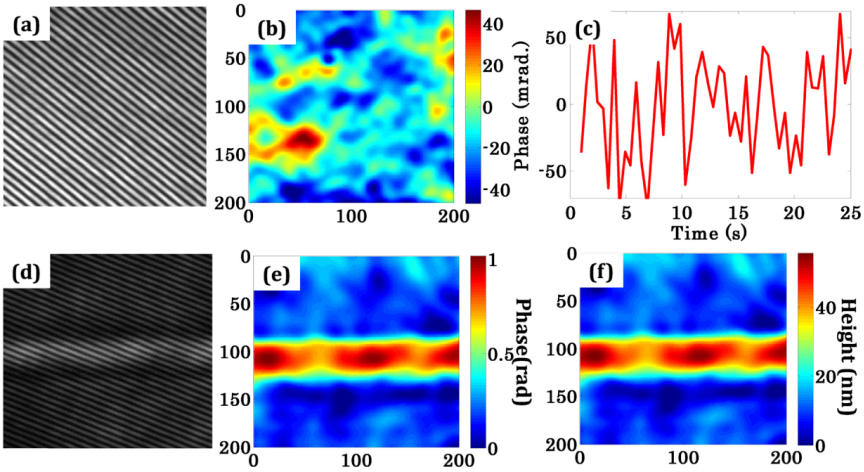

Fig. 2. Measurement of the spatial and temporal phase sensitivity of QPM while employing on the standard mirror (a) Interferogram obtained while using standard flat mirror as a test specimen (b) spatial, and (c) temporal phase noise of the experimental setup, (d) Interferogram of standard strip waveguide of 50 nm height, (e) phase image and (f) corresponding recovered height map which is approximately 50nm.

Optics EXPRESS

4.2 Multimodal imaging of MCC13 and macrophages

To demonstrate the multi-modal capability of the setup, sequential imaging of MCC13 cells was carried out, first with TIRF mode and then followed by QPI. The cell membrane was labeled with CMDR for the TIRF imaging. TIRF images were recorded using a laser operating at 660 nm wavelength and coupled into a waveguide of width 50 μm. After the TIRF images, the excitation laser were switched off and the interferograms of the same sample were recorded using He-Ne laser (using QPI mode). A water immersion (WI) objective lens (60X, 1.2 N.A. WI) was employed for imaging. Figure 3 shows different imaging modalities of the proposed experimental setup. Figure 3(a) and 3(b) compares the epi-fluorescence and TIRF images of the MCC13 cells respectively, and Fig. 3(c) shows the phase map of the same cell. For epi-fluorescence image (Fig. 3(a)) the sample was illuminated from the objective lens (MO_3), while for TIRF images the sample was illuminated by the evanescent field of the waveguide. It can be observed from Fig. 3(a) and 3(b) that the TIRF image provides excellent optical sectioning enhancing the contrast of the specimen's part that is close to the waveguide surface (Fig. 3(b)). The adhesion points of MCC13 (Fig. 3(b)) are visualized with high-contrast in TIRF module as compared to the epi-fluroscence image due to the optical sectioning provided by the exponential decaying evanescent field from the waveguide surface. The QPI module maps the phase variation of the same cell (Fig. 3(c)). The blue color in the phase image corresponds to zero phase shift introduced by the sample and deep red is for the maximum phase shift (Fig. 3(c)). The filopodia observed in TIRF image (Fig. 3(b)) are not visible in phase image (Fig. 3(c)) possibly because these features having their height less than the phase noise of the system.

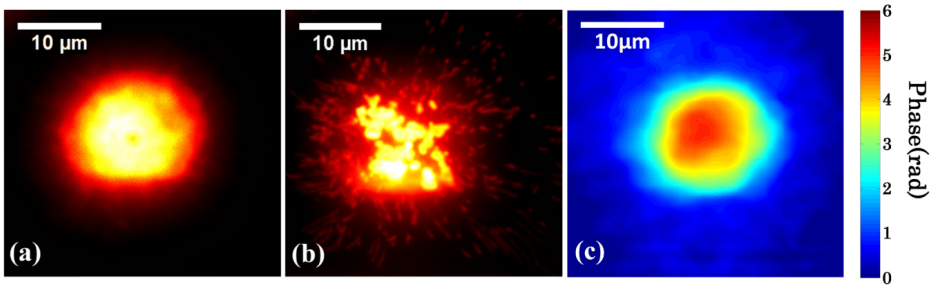

Fig. 3. Multi-modal imaging of a CMDR-labeled MCC13 cell. (a) Epi-fluorescence image, (b) chip-based TIRF image, and (c) 2D phase map of the same cell.

In contrast to conventional TIRF microscopy, this waveguide chip-based TIRF setup does not require a special high magnification TIRF objective lens (typically 60-100X) that limits the FOV to about 100 x 100 μm^2. The decoupling of the illumination and collection light paths allows using an objective lens with any desired magnification as the waveguide chip generates the evanescent field illumination independently. A 50 μm wide waveguide used in this work is multimode waveguide that support several modes inside the waveguide. These modes further interfere generating non-uniform evanescent field leading to non-uniform illumination as shown in Fig. 4(a). To produce uniform TIRF-M images, average of several images with different illumination patterns generated by different set of waveguide modes. This is achieved by horizontally translating (along the x-axis) the coupling objective MO_1 with a small step size of 50 nm and by acquiring a new image with every step. As the coupling objective is translated horizontally, a new set of modes are generated and illuminate the sample. A large number images ~250 are acquired. These set of images are then averaged on the intensity basis to obtain uniform TIRF-M image as can be seen in Fig. 4(b) and the associated Visualization 1.

Optics EXPRESS

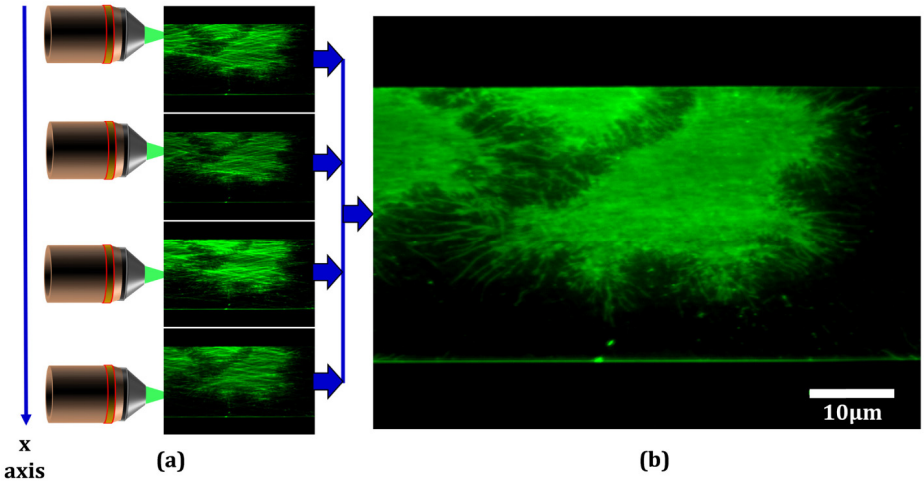

Fig. 4. Excitation of multiple modes inside the optical waveguide, which show generation of non-uniform evanescent field and thus resulting in non-uniform illumination of the specimen (a) Fluorescence images at different position of coupling objective by translating along x axis and (b) Resulting TIRF image obtained from superposition of 250 images by averaging them on intensity basis. Associated Visualization 1.

Figure 5 shows the TIRF and QPI images over extra-ordinary large FOV. Macrophages were labeled with CMG and laser @ 480 nm wavelength was used for these experiments. Figure 5(a) shows TIRF images of the macrophages acquired with 5X (0.1 NA) magnification over a large FOV of 1.32 x 1.32 mm^2 excited using the evanescent field of the waveguide. The white dotted line in Fig. 5(a) highlights the width of the waveguide (50 µm) and white arrow shows the direction of light propagation in waveguide. The cells present on the top of waveguide surface are selectively illuminated by the evanescent field. The region of interest can be imaged with high magnification by simply opting for a different imaging objective lens (e.g. 20X and 60X magnification) without influencing the illumination light path of the TIRF module. Figure 5(b) and 5(c) show TIRF and QPI images using a 20X (0.41 NA) magnification objective lens and Fig. 5(d) and 5(e) show images of the selected region using an objective lens of 60X (1.2 NA W.I.) magnification. The filopodia (villi-like projections) in the cell membrane of the macrophages are imaged with high contrast in the TIRF module (Fig. 5(d)). Figure 5 demonstrates the capability of the system to acquire both TIRF images and quantitative information about the morphological features of the cells over scalable magnification.

The optical waveguide structure introduces an unwanted constant phase offset to the phase values of cells, which was removed to determine quantitative phase measurements of the macrophages. The waveguide used in this work added a background phase of ~2 radian to the specimen, which was almost constant throughout the FOV of the objective lens. The constant phase generated by the waveguide was numerically subtracted for the accurate phase measurement of macrophages. Moreover, only those cells that were located completely on top of the waveguide structure were considered for all the phase measurements of controlled and inflammated macrophages. The cells that are present at the edges of waveguide, i.e. partially on top of waveguide and partially on the substrate were not considered for the calculation of the maximum phase values and subsequently for the whisker box plot.

Optics EXPRESS

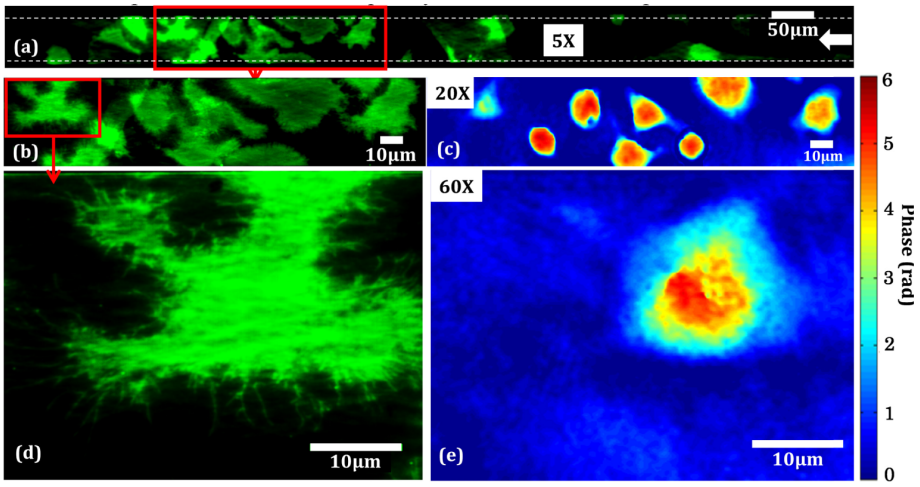

Fig. 5. (a) Waveguide-chip illumination enables TIRF imaging of CMG-labeled macrophages over extraordinarily large field of view (5X magnification). TIRF and phase images of the same selected region of interest with (b-c) 20X magnification and (d-e) with 60X magnification objective lenses respectively. As TIRF illumination is provided by the waveguide-chip, the illumination light path of TIFR and phase modules are decoupled, enabling easy switching between the objective lens of different magnification. The arrow in (a) show the direction of light coupling.

4.3 Investigating inflammatory response of macrophages

The proposed multi-modal microscopy was employed to detect the changes in morphology and functional features of macrophages when challenged by inflammatory molecules. All the experiments were performed on live cells and the effect of the inflammation on macrophages was studied using both TIRF and QPI modules sequentially. Inflammation was induced on the macrophages by incubating them for 24 hours with 10 µg/mL lipopolysaccharide (LPS). LPS is present on the outer membrane of gram-negative bacteria [34] that induces inflammation by stimulating the immune system, particularly in macrophages [36]. In response to these stimuli, pro-inflammatory cytokines and the inflammatory modulators are released which are known to cause inflammation or infection. As LPS is known to induce cellular stress in macrophages, it is possible that these might cause sub-cellular changes. We investigated the morphological and sub-cellular changes in control (unchallenged) and in LPS-challenged macrophages using the proposed multi-modal microscopy setup.

Figure 6(a) and (b) shows the TIRF and phase map for unchallenged macrophages, respectively. For the TIRF imaging, the cell membrane of the macrophages was labeled with CMG. In Fig. 6(a) the boundaries of the cell membrane and filopodia structures present on the plasma membrane are imaged in TIRF mode. The quantitative phase map of the same cell was obtained using the phase module of the set-up as demonstrated in Fig. 6(b). Figure 6(c) and (d) show the results of the LPS-challenged macrophages. The TIRF image in Fig. 6(c) highlights that LPS-challenged macrophages loose cell membrane integrity, with cell boundaries being disconnected at several locations. In addition, LPS-challenged macrophages possess fewer filopodia as compared to the control cells in Fig. 6(a). Using the QPI modality, i.e. by comparing Fig. 6(b) with Fig. 6(d) it was observed that the phase of the LPS-challenged macrophages decreases. The maximum phase of the normal and the LPS challenged macrophages are found to be 6.46 ± 0.61 rad and 5.11 ± 0.56 rad. The maximum phase values of the cells in this plot were calculated by taking the average of all pixels with a value of ≥90% of the maximum phase value for that cell. The decrease of the maximum phase of the LPS challenged macrophages suggests a decrease in the optical path length,

Optics EXPRESS

corresponding to either a decrease of the refractive index and/or decrease of thickness of the challenged macrophages. The phase images provide quantitative information about the morphological changes and the TIRF images provides information about the morphological changes of the cells due to inflammation caused by the LPS.

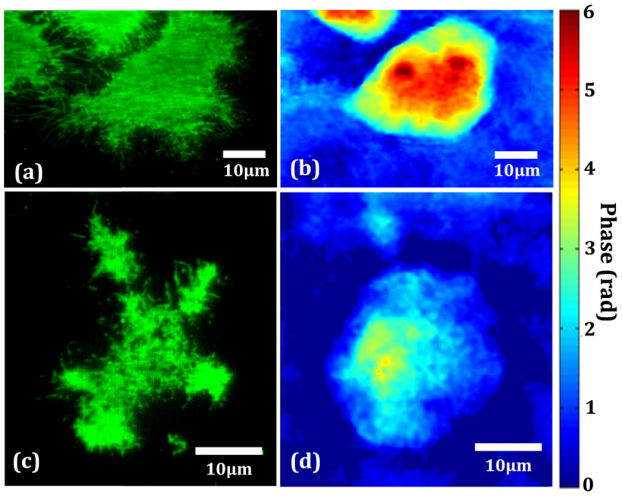

Fig. 6. (a) TIRF image and (b) quantitative phase image of unchallenged macrophages. (c) TIRF and (d) quantitative phase image of LPS-challenged macrophages.

To obtain statistically relevant data on quantitative phase, several sets of experiments were performed and over 1000 cells were analyzed. A similar trend, i.e. a decrease in the maximum phase value of the LPS-challenged macrophages was observed as compared to the normal unchallenged cells. A decrease in the maximum phase of the LPS-challenged macrophages indicates either a decrease in the refractive index of the cellular material or a reduction of cell thickness (flattening), or a combination of the two factors. Figure 7 shows the whisker box plot of the maximum phase values of the normal and LPS challenged macrophages. The first box is corresponding to the control (unchallenged) macrophages while second box is corresponding to macrophages after LPS inflammation. The average phase shift generated by the control cells was 6.46 ± 0.61 rad, compared to 5.11 ± 0.56 rad for LPS-challenged cells.

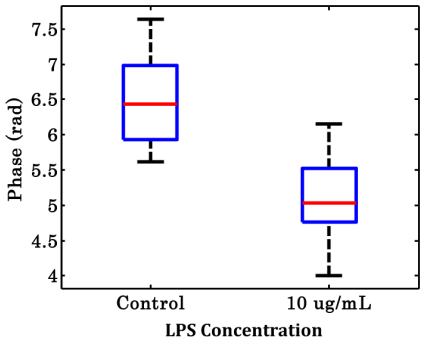

Fig. 7. Whisker box of maximum phase of the control and the LPS-challenged macrophages obtained by processing over 1000 macrophages. The central red lines indicate the median, and bottom and top sides of blue box indicate the 25th and 75th percentiles, respectively. The black lines extended vertically from blue boxes specify extreme data points without outliers

Optics EXPRESS

5. Conclusion

Here we developed a multi-modal microscope, by integrating chip-based TIRF microscopy with a Linnik-type QPI. This multi-modal microscope merges the individual advantages of TIRF microscopy, such as excellent optical sectioning, low photo-toxicity and high-contrast images, together with the quantitative expression of the cellular physiology and morphology provided by QPI. Such multi-modal imaging can be applied to the cellular structures or the biological processes that are present close to the cell membrane, such as membrane trafficking, membrane fenestrations, focal adhesion points, and nuclear pore complexes. Waveguide chip-based TIRF microscopy possess several advantages over conventional lens-based and prism based TIRF microscopy, including that the generation of the evanescent field is independent of the collection objective lens and multimodality, thus enabling TIRF imaging over an extraordinarily large FOV. By opting for an objective lens of lower magnification, the set-up enables the possibility to screen large cell populations in TIRF module and then performing QPI and TIRF microscopy of the region of interest with an objective lens of higher magnification. Development of an integrated chip-based TIRF microscopy and QPI is flexible towards future integration with other photonic chip-based optical systems, such as on-chip sensing, nanoscopy, particle tracking and trapping. It is also possible to decouple the geometrical height and RI of the biological cells by changing the media using microfluidics which is fully compatible with integrated chip platform. The proposed multi-modality TIRF and QPI system could be useful for broad range of applications where sensitive redistribution of sub-cellular content and organelles compared to the changes in the cell membrane surface are of interest. In particular, applications such as looking at overall cell morphology during uptake events for e.g. does a cell change its height while moving along the surface or during endocytosis, investigation of cell membrane protein-protein interactions when stimulated with different chemicals of interest.

The multi-modal microscopy was applied for imaging of living MCC13 cells and macrophages. In addition, the set-up was also employed to study the influence of LPS inflammation on macrophages. The artefacts in the plasma membrane of LPS challenged macrophages were observed with high contrast in the TIRF module; while the changes in the sub-cellular content of the macrophages was quantified by the QPI module. The results together suggest that LPS challenged macrophages losses the cell membrane integrity and decrease the maximum phase values. For the chosen concentration of LPS (10μg/ml), a rather significant difference in maximum phase value (21%) of the inflammated macrophages as compared to the normal macrophages was found (Fig. 7). it is therefore encouraging to further investigate the usefulness of the proposed technique for the diagnosing the inflammation in the macrophages. The proposed approach can be utilized for the quantitative assessment of health and infection of macrophages and other biological cells.

Funding

European Research Council (ERC) (336716); Norwegian Centre for International Cooperation in Education (SIU) (INCP-2014/10024); University Grant Commission (UGC).

Acknowledgments

B.S.A acknowledges the funding from the European Research Council, (project number 336716) and Norwegian Centre for International Cooperation in Education, SIU-Norway (Project number INCP- 2014/10024). D.S.M acknowledges University Grant Commission (UGC) India for joint funding.